ELSEVIER

Journal of Hydrology 245 (2001) 118–136

Journal of Hydrology

www.elsevier.com/locate/jhydrol

The seasonal water and energy exchange above and within a boreal aspen forest

P.D. Blanken[a,*], T.A. Black[b], H.H. Neumann[c], G. den Hartog[c], P.C. Yang[b], Z. Nesic[b], X. Lee[d]

[a]*Department of Geography and Program in Environmental Studies, University of Colorado, 260 UCB, 110 Guggenheim, Boulder, CO 80309 0260, USA*

[b]*University of British Columbia, Vancouver, BC, Canada*

[c]*Meteorological Service of Canada, Downsview, Ont., Canada*

[d]*Yale University, New Haven, CT, USA*

Received 21 August 2000; revised 10 January 2001; accepted 2 February 2001

Abstract

The seasonal water and energy exchange of a boreal aspen forest underlain by a hazelnut understory is described. Measurements of above-aspen latent and sensible heat, short-wave and net radiation, and photosynthetically active radiation are compared to those measured above the hazelnut understory. Understory radiation measurements were made using a tram system. Energy storage at each measurement height was determined, and measurements of the soil moisture, temperature, and heat flux were made using an array of probes.

The mean annual air temperature and total precipitation during 1994 were 1.2°C and 488.4 mm, respectively, above the 1951–1980 average −0.2°C and total 462.6 mm. There was a pronounced seasonal development of leaves, with the maximum leaf area index of the hazelnut (3.3 $m^2 m^{-2}$) exceeding that of the aspen (2.3 $m^2 m^{-2}$). Beneath-aspen radiation decreased exponentially as the aspen leaf area increased, and the calculated effective extinction coefficients decreased as the plant area index increased. At full aspen leaf, 27, 23, and 20% of the above-aspen short-wave, net, and photosynthetically active radiation, respectively, reached the hazelnut. The diurnal energy balance at both heights showed pronounced seasonal trends. Sensible heat from the forest floor dominated during the leaf-free period, whereas latent heat from the overstory dominated during the leafed period. The fraction of the annual precipitation evaporated was 82–91%, with 67–68%, 26–28%, and 4–7% originating from the aspen, hazelnut, and soil, respectively. Over the leafed period, soil water was depleted from the root zone (0–60 cm depth) and accumulated between the 61–123 cm depth, overall resulting in a deficit of 34.7 mm between 0–123 cm depths. This soil water balance compared well with the daily integrated difference between precipitation and eddy-covariance determined measurements of evaporation.

Keywords: Biometeorology; Boreal forest; Deciduous forest; Transpiration; Radiation; Surface energy balance

1. Introduction

The boreal forest's size, role in contemporary northern hemisphere climatology and global carbon cycle, and sensitivity to climatic change, were all reasons given to initiate the boreal ecosystem–atmosphere

* Corresponding author. Tel.: +1-303-492-5887; fax: +1-303-492-7501.

E-mail address: blanken@spot.colorado.edu (P.D. Blanken).

0022-1694/01/$ - see front matter
PII: S0022-1694(01)00343-2

study (BOREAS; see Sellers et al., 1997; Hall, 1999). At the southern edge of the boreal forest, deciduous aspen are found with a northern limit roughly corresponding to the 13°C July isotherm (Peterson and Peterson, 1992). Of the areas where *Populus* is the prominent genus, over 71% (ground area basis) occurs in the boreal forest region with 20–40% of Canada's aspen/poplar stands located in the prairie provinces (Peterson and Peterson, 1992). Aspen has been recognized as an economically important species with a variety of uses such as pulp, strandboard, lumber and plywood, fuel, shingle and shakes, etc. with harvesting recently increasing.

The deciduous nature of aspen demands that the energy and water exchanges be studied, if possible, over an entire season. The sparse and trembling nature of aspen crowns which is exaggerated by northerly locations often allows a sufficient amount of light penetration and the proliferation of understory species such as the hazelnut found at this study site. Whether the lush shrub understory found in aspen stands, in contrast to the moss and lichen layer with few shrubs typical of boreal conifer stands, is a result of the ample light penetration or due to the relatively higher nutrient status of *Populus* ecosystems is not clear. Exceptionally well-developed shrub understories, however, are typical under aspen stands (Peterson and Peterson, 1992). The extensive areal cover and relatively large leaf area of this understory species raises the question of how important the understory is relative to the overstory in terms of water and energy exchange. The deciduous nature of the hazelnut understory recommends that measurement here should also be made throughout an entire growing season.

An appreciation of the role that the forest understory or forest floor plays in the climatology of a forest has steadily increased over the past 30 years. Recent improvements in fast-response, robust sonic anemometers and scalar sensors have freed researchers from having to rely on flux-gradient approaches within canopies and the many theoretical and practical reservations associated with this approach. Today, most researchers routinely include beneath-canopy flux measurements as part of their research program. Results consistently show that the forest floor plays a significant role in terms of the whole stand, yet this role often varies considerably between site and seasons (e.g. Baldocchi et al., 2000; Constantin et al., 2000; Wilson et al., 2000). Presently, there are no long-term studies to conclusively show if there are also interannual trends or variability.

Previous work at this site has quantified the influence of the aspen architecture on radiation penetration (Chen et al., 1997), canopy conductance (Blanken et al., 1997), and carbon (Yang et al., 1999), and modeling studies have demonstrated the need for within-canopy measurements to complement those above canopy in order to better parameterize the models (Grant et al., 1999; Gu et al., 1999). No studies, however, have used simultaneous measurements at both the overstory and understory levels to explicitly describe the seasonal water and energy exchange.

The ambient conditions experienced during the 1994 BOREAS intensive study period (air temperature, precipitation, soil water content, leaf growth) are first described since this study is specific to the conditions experienced in one year. This is followed by micrometeorological details concerning the areal extent of tower measurements (i.e. fetch or flux footprints). The effect of leafing on radiation penetration is shown followed by description of the energy balance above and within the canopy for a typical day in each month from April through September. The seasonal playoff between sensible and latent heat is illustrated and the paper concludes with an analysis of the seasonal water balance.

2. Site description

The study site (53.6° N 106.2° W) is located in Prince Albert National Park, approximately 50 km NNW of Prince Albert, Saskatchewan, Canada, near the southern edge of the boreal forest. An even-aged stand of trembling aspen (*Populus tremuloides* Michx.) with scattered balsam poplar (*Populus balsamifera* L.) with a mean canopy height of 21.5 m and a stem density of 830 stems ha^{-1} developed after fire 70 years ago on mineral soils with 8–10 cm of organic material. Beneath a well-defined crown limited to the upper 5–6 m, was branchless trunk space. Hazelnut (*Corylus cornuta* Marsh.) with a mean canopy height of 2.0 m formed the understory, with wild rose (*Rosa woodsii*) and alder (*Alnus crispa*)

found intermittently. For all species, the average rooting depth was found to be approximately 60 cm. This predominantly aspen–hazelnut cover extended for at least 3 km in all directions.

3. Materials and methods

3.1. Above- and within-canopy eddy flux measurements

Measurements of the latent (λE) and sensible (H) heat fluxes above the aspen canopy ($z = 39$ m) and above the hazelnut understory canopy ($z = 4$ m) were made using the eddy-covariance technique. To summarize, the three components of wind velocity (vertical, lateral and longitudinal) and air temperature were measured at each level at 20 Hz with sonic anemometer–thermometers. The water vapor and CO_2 mole fraction scalars were measured with infrared gas analyzers located at each level. Turbulent scalar eddy fluxes were calculated for each 1/2 h as the covariance between the vertical wind speed (w) and the scalar x ($\text{flux} = \text{cov}(w,x) = \overline{w'x'} = \overline{(w - \bar{w})(x - \bar{x})}$), where the prime denotes deviation from the 1/2 h mean (overbar). Instruments were mounted on two scaffold-type towers, one 6 m tall and the other 37 m tall. Turbulent fluxes away from the surface were considered positive, and towards the surface negative. Full details on the eddy flux measurements can be found in Black et al. (1996), and Blanken et al. (1997, 1998).

3.2. Above-canopy radiation measurements

Net radiation (R_n) (model S-1, Swissteco Instruments, Oberriet, Switzerland and model CN-1, Middleton Instruments, Melbourne, Australia), incident solar radiation (direct and diffuse, $R_s\downarrow$) (model PSP, Eppley Inc., Newport, RI) and incident photosynthetically active radiation ($Q_p\downarrow$) (model 190-SB, LI-COR Inc., Lincoln, NB) were measured at 33 m above the ground on the main tower. The net radiometers were supported at the end of a 3 m long horizontal boom extending south of the tower. All signals were recorded on dataloggers (models 21X and 7X or CR7, Campbell Scientific Inc. (CSI), Logan, UT).

Prior to installation in February 1994, both net radiometers were calibrated at the Atmospheric Environment Service (AES) radiation laboratory facility in Downsview, Ontario. At the end of the 1994 field season, the Swissteco radiometer was sent back to the AES laboratory where the sensitivity ($\text{W m}^{-2}\,\text{mV}^{-1}$) was found to be less than 2% above the pre-field season calibration.

In-situ short-wave calibration was performed on April 11 and September 19, 1994. During clear-sky conditions, the Eppley pyranometer and the net radiometers were simultaneously shaded with small shades 2 m from the sensors in order to minimize the effect of incident diffuse long- and short-wave radiation from the shade itself. The ratio of the drop in Eppley short-wave radiation to the drop in the net radiometer's millivolt output was compared to the AES calibrations. These experiments revealed that in contrast to the pre-field laboratory calibrations, the Swissteco was overestimating $R_s\downarrow$ by a mean 3% while the Middleton was underestimating $R_s\downarrow$ by a mean 9%.

An in-situ evaluation of the net radiometers was performed (Hodges and Smith, 1995) by placing a net radiometer (model Q*1 (Fritschen), Radiation Energy Balance Systems, Seattle, WA) beside the Swissteco and Middleton net radiometers for a three-day period in July 1994. This evaluation showed that for $R_n \geq 0$, the Swissteco and Middleton R_n measurements were 3 and 8% lower than the REBS, respectively, in good agreement with the in-situ short-wave radiation calibration for the Middleton but slightly at odds for that of the Swissteco. Based on the results of the in-situ calibration, the consistency of the laboratory calibration as well as its short time constant, the overstory R_n reported here is from the Swissteco reduced by 3% from the original AES laboratory calibration.

3.3. Within-canopy radiation measurements

Measurement of the radiation regime beneath a canopy is difficult due to spatial heterogeneity, yet its determination is crucial for a complete understanding of within-canopy energy balance processes. By the nature of a forest overstory canopy, radiation levels can change quickly from full above-canopy values to almost zero due to fluttering leaves, flexible trunks and canopy gaps, and vary diurnally due to changes in the radiation beam path length with solar

Table 1
Approximations for total heat storage between 0–39 m or 0–4 m using a linear equation $J_t(\mathrm{W\ m^{-2}}) = ax + b$, where x is the 1/2 h change in air temperature (ΔT_a°C) or net radiation (ΔR_n W m^{-2}) measured above the aspen canopy and a and b are empirical coefficients (equations are independent of the time of year or day)

Height interval (m)	a (W m^{-2}/°C or W m^{-2}/W m^{-2})	x (°C or W m^{-2})	b (W m^{-2})	r^2	n (1/2 h)
0–39	44.5	ΔT_a	1.66	0.85	7962
0–39	0.10	ΔR_n	−7.4	0.71	7962
0–4	7.0	ΔT_a	0.70	0.83	8053
0–4	0.02	ΔR_n	−1.59	0.78	8053

azimuth. This often precludes the use of stationary radiation sensors beneath the canopy. For example, to detect to within 10% a forest floor solar irradiance of 200 W m^{-2} (using statistical α and β parameters of 0.95 and 0.90, respectively) in a homogeneous overstory canopy (variance in forest floor $R_s\downarrow$ of only 10 W m^{-2}) would require 10 samples or 10 stationary pyranometers. The variance in $R_s\downarrow$ beneath the aspen canopy was typically 51 W m^{-2} (clear-sky conditions) so a minimum of 20 stationary pyranometers would be required under the aspen canopy to reasonably measure understory solar radiation.

To overcome this inherent impractical problem, $R_s\downarrow$, $Q_p\downarrow$ and R_n were measured by individual sensors as the average of 900 samples taken on a tram platform moving along a horizontal distance of 60 m over a duration of 15 min (equivalent to 30 samples every meter at a velocity of 7 cm s^{-1}). The tram was suspended on two parallel steel cables 4 m above the ground and carried two net radiometers (models S-1 and S-14 miniature, Swissteco Instruments), up-facing and down-facing quantum sensors (model 190-SB, LI-COR, Lincoln, NB) and two up-facing pyranometers (one shaded) (model CM-5, Kipp and Zonen Laboratory, Delft, The Netherlands). Data were recorded by a datalogger (model CR10, CSI) carried onboard the tram. Magnetic switches located at both ends of the tramway were activated by magnets on the tram and sent a signal to reverse a 1/4 hp DC motor which pulled the tram with a fine-steel cable.

3.4. Energy storage

The total rate of energy storage in a column extending from the ground surface to either the 4 or 39 m height was calculated as $J_t = J_b + J_l + J_h + J_e + J_p$ where subscripts b, l, h, e and p are the rates of change of heat content in the boles (stems), leaves, sensible heat content in the air column, latent heat content in the air column and energy consumed for photosynthesis, respectively. These were measured using a transect of thermocouples through the bole of an aspen tree and one in a hazelnut stem, infrared thermometers aimed at each canopy, an air temperature profile (as described by Lee and Barr, 1998), and humidity and CO_2 profiles. Full details on how each of these energy storage components was calculated is given in Blanken et al., 1997. Due to the complexity involved in fully instrumenting all components of the total storage terms, the linear equations derived from linear regressions are given as useful approximations using readily available measurements of T_a or even R_n (Table 1).

3.5. Soil heat flux, water content and evaporation

The soil heat flux (G) at a depth of 3 cm was measured with a 20 m transect of nine heat flux plates (two model F, Middleton Instruments; seven home-made following Fuchs and Tanner, 1968) recorded on a datalogger (model CR7, CSI). The surface soil heat flux (G_0) was calculated by adding G at the 3 cm depth to the 0–3 cm rate of heat storage (i.e. $G_0 = G + C_s\Delta T_s/\Delta t$, where C_s is the volumetric heat capacity in the top 3 cm of organic soil and $\Delta T_s/\Delta t$ is the half hourly temperature change in the top 3 cm). The volumetric heat capacity was calculated as $C_s = \theta_m C_m + \theta_o C_o + \theta_w C_w + \theta_a C_a \approx \theta_o C_o + \theta_w C_w$, where θ_m, θ_o, θ_w and θ_a are volumetric fractions of minerals, organic matter, water and air. A typical C_o and C_w of 2.50 and 4.18 MJ m^{-3} °C^{-1} (respectively) were used (Hillel, 1982) and θ_o was

calculated as $\theta_o = \rho_b/\rho_o$, where ρ_b (measured as 160 kg m^{-3}) and ρ_o (typically 1300 kg m^{-3}; Hillel, 1982) are the organic soil dry bulk and particle densities, respectively. The volumetric water content (m^3 water m^{-3} soil) in the 0–3 cm layer (θ or $\theta_w = w\rho_b/\rho_w$) was determined from the gravimetric soil water content w (kg water kg^{-1}dry soil) (see next paragraph). The average temperature change per 1/2 h in the 0–3 cm layer was determined by two home-made integrating thermometers (nickel wire wound around a glass cylinder and coated with epoxy) inserted diagonally across the 0–3 cm depth.

The soil water content was determined at several depths through the soil profile by two methods. To ensure correct measurement of C_s, w was measured gravimetrically every two to three days with soil samples obtained over the 0–3 cm, 3–6 cm and start of mineral soil to 10 cm layers. Each sample was oven-dried at the site at 105°C for at least 24 h with w calculated as the difference between the fresh and oven-dried weights relative to the dry weight. This method was complimented with the time-domain reflectrometry (TDR) technique (Topp et al., 1980) which permitted measurements of θ with absolute errors of 0.023–0.034 m^3 m^{-3} (Hook and Livingston, 1996).

In the fall of 1993, two probes consisting of three stainless steel rods (3 mm diameter, 30 cm long, 2 cm apart) were positioned horizontally in the middle of the local organic (8 cm depth) and mineral (15 cm depth) horizons. A 123 cm rod (two stainless steel strips 2 cm apart separated by epoxy) was also installed to measure θ at depths integrating over 30.5 cm segments. Both the probes and the rod used the shorting-diode technique (Hook et al., 1992) and θ was calculated from the delay times using the algorithm of Hook and Livingston (1996). The delay times were measured using cable-length testers (models 1502B and C, Tektronix, Beaverton, OR) with a resolution of 0.004 m^3 m^{-3}. The gravimetrically determined θ for the 3–6 cm layer was used to calibrate the 8 cm TDR probe ($\theta_{TDR} = 0.48\theta_{grav.} + 0.049$; $r^2 = 0.69$; $n = 52$).

To gauge soil water evaporation, two small thin-walled plastic lysimeters (15 cm diameter and 15 cm deep) were installed in late July. The lysimeters were weighed manually every 2 h to the nearest 0.1 g (model P3, Mettler Instrument Corp., Princeton, NJ) during the day for a 15-day rain-free period. To prevent drying out of the soil in the lysimeters and hence decoupling from the surrounding soil, the soil was replaced after five to seven days following the suggestion of Boast and Robertson (1982). These measurements were used to estimate soil evaporation at other times using the ratio of soil evaporation to forest evapotranspiration.

3.6. Precipitation

Precipitation was measured half hourly in the center of a clearing (approximate diameter 75 m) located roughly 200 m from the main tower. Precipitation in the form of snow was measured with a Nipher-shielded weighing precipitation gauge (Belfort Instruments, Baltimore, MD). Precipitation in the form of rain was also measured with a tipping-bucket rain gauge (model TE525, CSI). Periods of missing data were replaced by measurements obtained by an AES tipping-bucket or manual rain gauge located in an adjacent clearing.

3.7. Leaf, plant and wood area indexes

One-side (projected) leaf area index (LAI; m^2 projected leaf m^{-2} ground) was measured optically throughout the year using a LI-COR Plant Canopy Analyzer (model LAI-2000, LI-COR Inc., Lincoln, NB). Since this instrument requires diffuse solar radiation conditions, readings were taken either on overcast days, or just before or after sunset. To isolate the aspen canopy, readings were made at the 25 m height from the walk-up tower and at the 3 m height (i.e. above the hazelnut) at two pre-determined locations. Hazelnut canopy measurements consisted of pairs of below and above hazelnut readings taken at six pre-determined locations along a 100 m east–west transect within the flux footprints of the towers (see below). The same locations were used throughout the year. A wood (boles and branches) area index (WAI) of 0.62 (aspen) and 0.34 (hazelnut) was determined from measurements taken before leafing and the LAI was calculated by subtracting WAI from the plant area index (PAI). LAI values were also corrected for clumping (seasonally adjusted for the aspen canopy; see Chen et al., 1997, for details) and blue-light scattering. Forest LAI was calculated as the sum of aspen and hazelnut LAI.

3.8. Fetch or flux footprints

The one-dimensional footprint from a measurement made at a height z at an upwind distance x normalized by the flux Q is given as

$$(1/Q)dQ/dx = [U(z-d)/(u^{*}\mathrm{k}x^{2})] \times \exp[-U(z-d)/(\mathrm{k}u^{*}x)] \quad (1)$$

(Schuepp et al., 1990; Eq. (9)) where d is the zero-plane displacement (well approximated by $2/3h_c$; Brutsaert, 1984), k is the von Karman constant, u^{*} is the friction velocity and U is height-averaged (4 or 39 m) wind speed given as

$$U = \frac{u^{*}[\ln((z-d)z_0 - 1 + z_0/(z-d))]}{\mathrm{k}(1 - z_0/(z-d))} \quad (2)$$

(Schuepp et al., 1990; Eq. (6)). The first derivative of Eq. (1) equated to zero yields the upwind horizontal distance to which the flux measurement is most sensitive (peak footprint) and is given as

$$x_{\max} = (U/u^{*})[(z-d)/2\mathrm{k}] \quad (3)$$

and the cumulative normalized contribution is the integration of Eq. (1) from 0 to x,

$$Q(x)/Q = \exp[(-U(z-d)/(\mathrm{k}u^{*}x))] \quad (4)$$

(Schuepp et al., 1990; Eqs. (10) and (13), respectively). Since flux footprints are affected by atmospheric stability (Leclerc and Thurtell, 1990), Eq. (1) was modified as suggested by Schuepp et al. (1990) to include these effects (U/u^{*} ratios multiplied by the stability correction for momentum of the forms suggested by Dyer, 1972). The stability corrections were calculated using the median $(z-d)/L$ (where L is the Obukhov stability length) during the daytime (-0.11 at $z = 39$ m and -0.28 at $z = 4$ m) and nighttime (0.26 at $z = 39$ m and 0.29 at $z = 4$ m) periods.

4. Results and discussion

4.1. Site conditions during 1994

The study site falls on the northern edge of the prairie climate region with mild, wet summers and cold, dry winters (Hare and Thomas, 1974). Fig. 1 shows the strong seasonality in both air temperature (T_a) and precipitation (P). Compared with the 1951–1980 long-term average T_a and P recorded at Waskesiu Lake (53.9° N, 106.1° W; Canadian Climate Normals, 1982), January and February were colder than the average, with several contiguous days well below the average, indicative of well-developed stationary high-pressure systems. The spring (March–April–May) was, however, slightly warmer than average with the trend of above-average temperatures continuing right though the summer into early fall (June–July–August–September). The remainder of the fall and winter experienced temperatures close to average except for December, which was much warmer. On an annual basis, the mean T_a of 1.2°C was significantly different from the average -0.2°C at the $p = 0.11$ level (student's t-test).

The annual precipitation cycle (Fig. 1) shows that during an average year, 45% of the annual P is delivered during the summer months (June, July and August). During 1994, the average annual P pattern was followed with the exception of a very wet May and June and a drier than average August and September. March and October also received more than the average P. The high May and June P was partially attributable to intense, local convective storms. On an annual basis, the February–December total P of

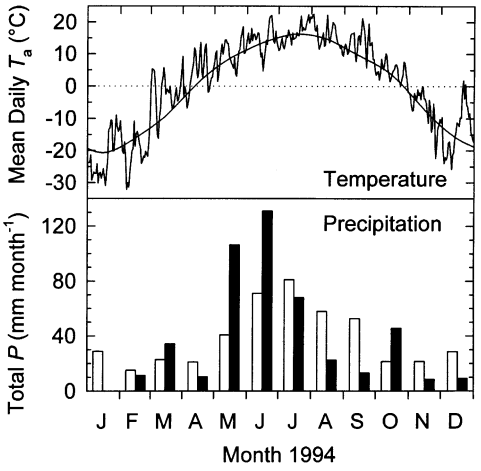

Fig. 1. Comparison of the daily mean air temperature (T_a) measured above the aspen forest at $z = 39$ m (jagged line), and the monthly total precipitation (P) measured in a clearing at the research site (solid vertical bars) to the 1951–1980 average T_a (smooth line) and monthly total precipitation (clear vertical bars) measured at Waskesiu Lake.

462 mm was above the 434 mm average during the same period (unfortunately, P instrumentation was not installed until late January). If it is assumed that the missing January P in 1994 was equal to the daily average amount for that month (29 mm January total), then the total P in 1994 (488 mm) was 25 mm above the 463 mm average.

The seasonal P patterns were somewhat reflected by the changes in the volumetric soil moisture content (θ) observed from TDR measurements made at several depths in the soil profile (Fig. 2) except during the spring thaw period. During the frozen winter period, measurements of θ remained stable at 6–13% in the organic, shallow mineral and 61–92 cm deep mineral layers, magnitudes similar to those reported by Hayhoe et al. (1983) in frozen soils. A substantially higher winter θ of 25% was measured deep in the profile where temperatures remained positive. Since TDR measurements made in frozen soils indicate the unfrozen water content (Hayhoe et al., 1983; Spaans and Baker, 1995), this suggested that there was some liquid water present, even during the coldest time of the year. In April, θ increased markedly in the organic and shallow mineral horizons despite relatively little precipitation. The relative contribution to this increase from the infiltration of snowmelt water (all snow melted by April 15) and the melting of ice in the soil (soil temperature at the 2, 5 10, 20 and 50 cm depths reached 0°C by April 17, 18, 21, 23 and 29, respectively) was not known. The fact that there was no spring-time increase in θ in the deep mineral soil and soil temperature at 100 cm depth was always positive (annual minimum of 0.05°C reached between April 1–21) confirmed that there was little frozen water at this depth over the winter and suggested that infiltration of snowmelt water did not reach deep into the soil profile.

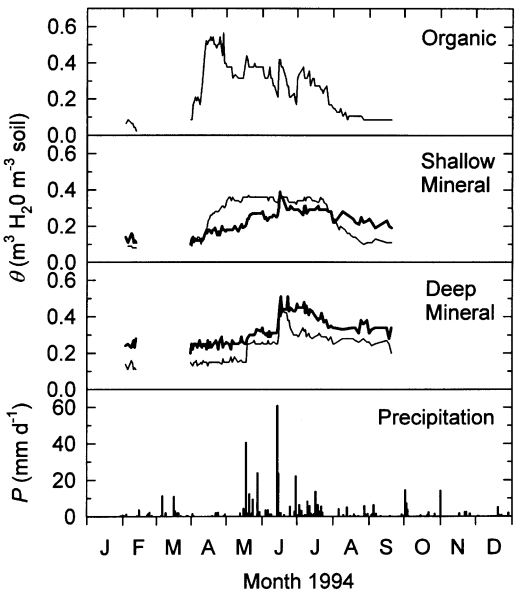

Fig. 2. Seasonal course of daily volumetric soil moisture content (θ; lines) and precipitation (P; vertical bars). The organic layer (≈0–10 cm) was represented by a three-prong TDR probe inserted horizontally at a depth of 8 cm approximately in the middle of the organic horizon. The shallow mineral layer (≈ 10–30 cm) was represented by a three-prong TDR probe inserted horizontally at a depth of 15 cm (thin line) and the 30–61 cm section of a segmented TDR vertical rod (thick line). The deep mineral layer (≈ 61–123 cm) was represented by the 61–92 cm (thin line) and 92–123 cm (thick line) sections of a segmented TDR vertical rod.

Following the spring increase, θ gradually decreased through the season in the organic layer with intermittent responses to P events. In the shallow mineral layer, θ maintained its spring melt value of approximately 35%, showed little response to P events and did not decrease substantially until late July. The deep mineral layer showed a large increase following the moderately heavy July rainfall and slowly decreased thereafter. Both measurements of θ in the deep mineral layer showed a marked response to the substantial May rainfall after the relatively dry April.

Following snowmelt, bud-burst began and lasted until leaf emergence in the third week of May (Fig. 3). Aspen leaf emergence lasted until early June while leaf growth continued until a LAI of 2.3 was reached by mid-July. Seasonal variation in the timing of leaf emergence has been correlated to carbon sequestration (Black et al., 2000), and the total LAI was positively correlated to canopy conductance (Blanken et al., 1997). Branch loss and possible leaf curling slightly decreased the aspen LAI until senescence began in the second week of September. Similar to the aspen, hazelnut bud-burst began right after snowmelt with leaf emergence beginning in the third week of May. In contrast to the aspen, hazelnut leaf growth continued until late June with a maximum LAI of 3.3 exceeding that of the aspen was attained by July. Hazelnut senescence began approximately ten days

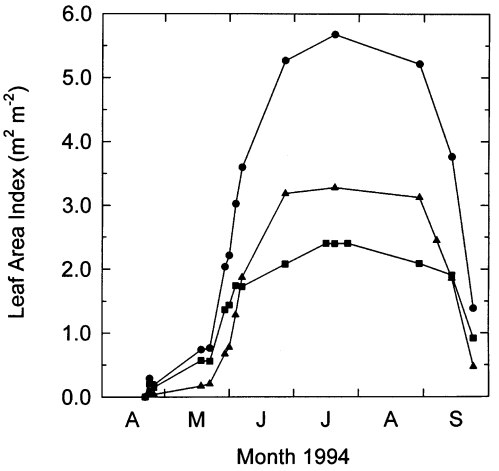

Fig. 3. Seasonal development of the forest (●), hazelnut understory (▲) and aspen overstory (■) leaf area indices. Maximum leaf area indices of 2.3, 3.3 and 5.6 m^2 leaf per m^2 ground were obtained by the aspen, hazelnut and forest, respectively.

before the aspen. Overall, the forest reached a maximum LAI of 5.6 by mid-July.

4.2. Footprint predictions of the flux source

The relative flux contribution as a function of upwind distance (flux footprint or fetch) at both measurement levels above and within the aspen canopy is shown in Fig. 4. The important feature of Fig. 4 is the distance at which the peak footprint occurs (x_{max}; upwind distance to which the flux measurements are most sensitive) and how this distance changed with typical diurnal variations in atmospheric stability.

Above the aspen canopy at $z = 39$ m, x_{max} under neutral conditions was 129 m. This contracted to 99 m and extended to 296 m under typical daytime and nighttime atmospheric stability conditions, respectively. Within the aspen canopy above the hazelnut understory ($z = 4$ m), the x_{max} was 15 m in neutral conditions and ranged from 10 to 37 m under typical daytime and nighttime atmospheric stabilities, respectively. Despite the relatively small values of x_{max} above the aspen canopy, the cumulative flux reached 80% of the total flux at an upwind distance of 1160 m under neutral conditions, 900 m under typical daytime stability conditions, and 2660 m under typical nighttime stability conditions (Fig. 5). Thus the fetch requirements (fetch: $z–d$ where 80% of the total flux was reached) were relaxed (47:1 and 36:1, during neutral and daytime conditions, respectively, and slightly extended at night (106:1) compared to the micrometeorological rule-of-thumb of 100:1, but the horizontal distances were quite large because of the high measurement height. Within the canopy at $z = 4$ m, the upwind distance required to reach 80% of the total flux was also well beyond the peak footprints. Distances of 135 m (neutral), 90 m (daytime) and 333 m (nighttime) or fetch: z/d ratios of 51:1, 34:1 and 125:1 (neutral, daytime and nighttime, respectively) were comparable to those above the forest.

4.3. Within-canopy radiation

To quantify the within-canopy radiation regime and to develop a simple empirical model of radiation extinction, the daytime means of the ratios of understory to overstory R_n, $Q_p\downarrow$ and $R_s\downarrow$ were plotted against aspen LAI (Fig. 6). Extinction of radiation through the canopy was largely a function of aspen LAI, and an exponential equation of the form $Q\downarrow$ (4 m)/$Q\downarrow$ (39 m) = $a\exp(-ba_l)$, where a and b are

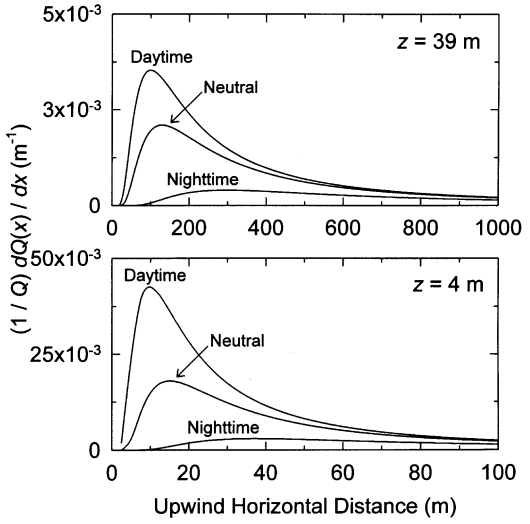

Fig. 4. The 'flux footprint' or relative contribution to the flux measured at $x = 0$ m ($1/Q_0 dQ(x)/dx$) as a function of the upwind distance x for $z = 39$ m and $z = 4$ m (area under each curve is unity). Neutral stability, typical daytime and nighttime footprints are shown. The latter were calculated by correcting for atmospheric stability using the median $(z - d)/L$ during daytime ($R_n > 0$ W m^{-2}) and nighttime ($R_n < 0$ W m^{-2}) periods.

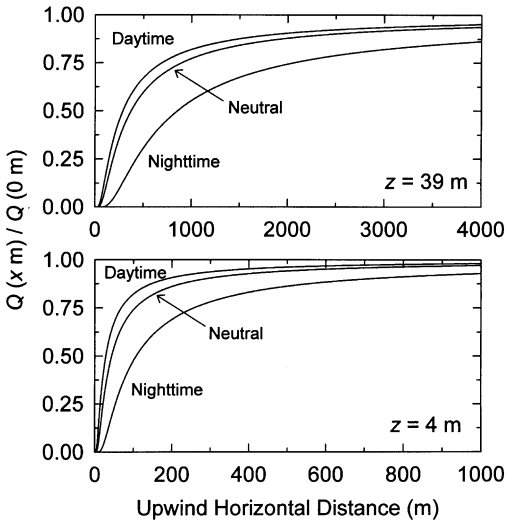

Fig. 5. The cumulative flux footprint or cumulative relative contribution at an upwind distance x ($Q(x)$) to the total flux Q measured at $x = 0$ m for $z = 39$ m and $z = 4$ m. Neutral stability, typical daytime and nighttime footprints are shown. The latter were calculated by correcting for atmospheric stability using the median $(z - d)/L$ during daytime ($R_n > 0$ W m^{-2}) and nighttime ($R_n < 0$ W m^{-2}) periods.

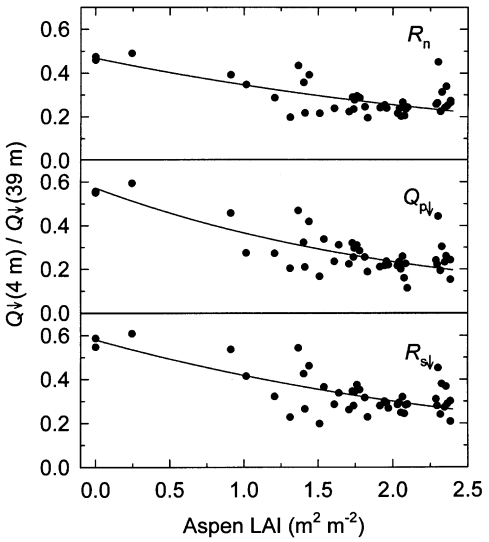

Fig. 6. Ratio of net radiation (R_n), photosynthetically active photon flux ($Q_p\downarrow$) and solar radiation ($R_s\downarrow$) measured above the hazelnut understory ($z = 4$ m) to that measured above the aspen ($z = 39$ m) plotted as a function of the seasonal development of aspen leaf area index (LAI). Points represent daytime means ($R_n > 0$ W m^{-2}) and the solid line represents a curve fit of the form $Q\downarrow$ (4 m)/$Q\downarrow$ (39 m) $= a \exp(-ba_l)$. See Table 2 for curve-fit parameters.

constants and a_l is the LAI, best described this relationship (Table 2). Without leaves, the ratios of below to above fluxes were greatest for $R_s\downarrow$ (0.58) and $Q_p\downarrow$ (0.57) followed by R_n (0.47). With leaves, ratios of $Q\downarrow$ (4 m)/$Q\downarrow$ (39 m) decreased significantly falling to 0.27 ($R_s\downarrow$), 0.23 (R_n) and 0.20 ($Q_p\downarrow$).

The exponential decrease in all three radiation components with increasing LAI implied that attenuation could be expressed using a form of the Beer–Bouger Law, $Q\downarrow(z) = Q\downarrow_0 \exp(-ka_p)$, where $Q\downarrow_0$ is the top of the canopy incident radiation, k is the effective extinction coefficient and a_p is the PAI ($a_p = a_l + a_w$, where a_l is the LAI and a_w is the WAI equal to 0.62 for the aspen). In strict terms, the Beer–Bouger Law describes the exponential attenuation of single-wavelength radiation with depth in a homogenous medium with complete absorption and no scattering. Its application with depth replaced by accumulated leaf or plant area (Monsi and Saeki, 1953) has surprisingly resulted in good descriptions of attenuation of broad radiation band widths in several plant canopies (Campbell and Norman, 1998).

Calculating k and plotting it as a function PAI is shown in Fig. 7. PAI was chosen over LAI since k cannot be calculated when $a_l = 0$. In general, k decreased suddenly following leaf out and then dropped only slightly during the full-leaf period. The fact that the best fit between $Q\downarrow$ (4 m)/$Q\downarrow$ (39 m) and LAI was exponential implies that a constant b (i.e. effective extinction coefficient) worked well as shown in Fig. 7. The decrease in k for all three radiation streams as PAI increased implied that although there was less radiation reaching the understory when the aspen canopy was mature, the radiation that did reach the understory did so more efficiently. This counter-intuitive result, also found in other deciduous forests (Rauner, 1976; Baldocchi et al., 1984), was likely due to the shorter radiation path

Table 2
Coefficients determined for the curve fit of the form $Q\downarrow$ (4 m)/$Q\downarrow$ (39 m) $= a \exp(-ba_l)$ as shown in Fig. 6

Radiation stream $Q\downarrow$	a	b	r^2	n (days)
R_n	0.4682	0.3038	0.74	44
$Q_p\downarrow$	0.5719	0.4450	0.76	44
$R_s\downarrow$	0.2910	0.3283	0.72	44

Table 3
Comparison of leafless and leafed deciduous forest canopy's effective extinction coefficients (k) expressed on a leaf and plant area index basis for net radiation (R_n), photosynthetically active photon flux ($Q_p\downarrow$) and solar radiation ($R_s\downarrow$)

Radiation stream	Leafless canopy k	Leafed canopy k	LAI	PAI	Reference
R_n	1.75	0.54	4.9	5.5	Baldocchi et al. (1984)
	1.62	0.47	3.5	4.0	Rauner (1976)
	1.22	0.49	2.3	2.9	This study
$R_s\downarrow$	1.12	0.51	4.9	5.5	Baldocchi et al. (1984)
	1.00	0.42	3.5	4.0	Rauner (1976)
	0.88	0.44	2.3	2.9	This study
$Q_p\downarrow$	1.06	0.66	4.9	5.5	Baldocchi et al. (1984)
	N/A	0.6–1.0	3.5	4.0	Rauner (1976)
	0.90	0.54	2.3	2.9	This study

lengths through the canopy in summertime when solar zenith angles were small and also due to beam enrichment resulting from forward scattering of light in the leafed canopy.

Comparing the effective extinction coefficients from the boreal aspen forest to other deciduous forests (Table 3), some general conclusions may be drawn. During the winter period with leafless canopies, $k(R_n) > k(Q_p\downarrow) \approx k(R_s\downarrow)$. Large solar zenith angles and long path lengths severely attenuated the shortwave component of R_n in addition to long-wave attenuation by the opaque branches and trunks while the absence of leaves precluded any possible trapping and re-radiating of long-wave radiation. For the bare canopy, $k(Q_p\downarrow) \approx k(R_s\downarrow)$ since there were no leaves present to absorb $Q_p\downarrow$ so both radiation streams were attenuated equally.

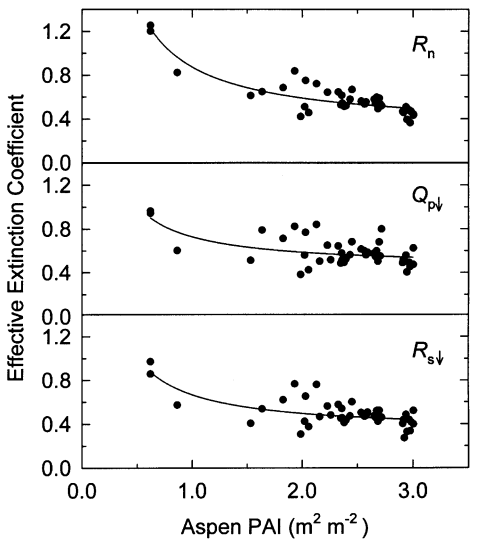

Fig. 7. Effective extinction coefficients (k) for net radiation (R_n), the photosynthetically active photon flux ($Q_p\downarrow$) and solar radiation ($R_s\downarrow$) derived from the equation $k = -\ln(Q\downarrow\ (4\ m)/Q\downarrow\ (39\ m))/a_p$, where a_p is the aspen plant area index, the sum of aspen leaf and wood area indexes. Solid lines represent k calculated using the equation $Q\downarrow\ (4\ m)/Q\downarrow\ (39\ m) = a\ \exp(-ba_l)$ obtained in Fig. 6.

As the leaves develop and reach maturity, $k(Q_p\downarrow) > k(R_n) \approx k(R_s\downarrow)$. Since leaves have a high absorptivity in the 400–700 nm waveband, $Q_p\downarrow$ was attenuated more than $R_s\downarrow$. As leaves are almost blackbodies, the long-wave portion of R_n suffered little attenuation, but the leaves absorbed and forward-scattered shortwave radiation, decreasing $k(R_n)$ from the winter values. The influence of this trapping, however, was probably not large since $k(R_n)$ values were similar to $k(R_s\downarrow)$ values.

4.4. Seasonal progression of the diurnal energy balance

To summarize diurnal patterns, ensemble averages of the energy balance components for each month for the forest (Fig. 8) and for the hazelnut understory (Fig. 9) were calculated at hourly intervals. To focus on the daytime period, energy balance components for the forest and understory standardized by R_n are given in Table 4.

4.4.1. Spring (April–May)

During the April–May leafless period, the striking feature of Fig. 8 is the large proportion of R_n utilized

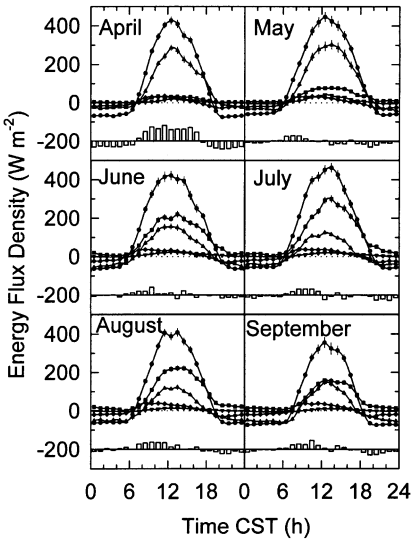

Fig. 8. Ensemble monthly averages of the forest ($z = 39$ m) diurnal net radiation (R_n, ●), latent heat (λE, ■, sensible heat (H, ▲), soil heat (G_0, ▼) and total heat storage (J_t, ◆) flux densities. Each data point represents the mean of 2 1/2 h periods with ±1 standard error of the mean shown by the vertical lines. The vertical bars represent the residual of energy balance closure, calculated as $R_n - \lambda E - H - G_0 - J_t$.

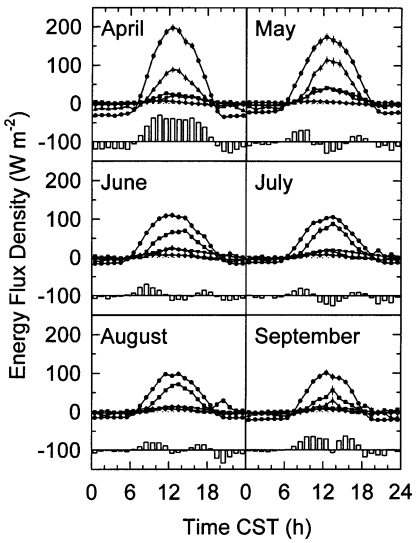

Fig. 9. Same as Fig. 8, except for at the understory ($z = 4$ m).

by H above the aspen canopy with typical daytime H/R_n ratios of 0.64. At the understory level, H was also the dominant component of R_n, but not as large as above the canopy and did not peak until May. The lack of leaves meant minimal λE contributions at both levels, with some soil water evaporation. With the frozen surface soil, G_0 during April was limited since energy was used for the phase-change from solid to liquid water before soil warming could occur (soil temperature at the 5 cm depth hovered around 0 °C between April 1–18, but increased dramatically afterwards, as a result of the melting frozen soil). We calculated that 6 W m^{-2} would be required, each hour, to melt this ice over this period. The soil heat flux reached its peak in May when the bare canopies allowed maximum $R_s\downarrow$ penetration resulting in steep soil temperature gradients (as much as 10°C over a depth of 2 cm) occurring in the leaf litter layer acting as a surface mulch. At the understory level, G_0 was of comparable magnitude to λE during the month of May. The total storage of heat within the canopy between 0–39 m height during the spring months was of comparable magnitude to G_0. The daytime mean 0–39 m J_t was partitioned equally between heat storage in the air column and boles. At the

Table 4
Ensemble daytime (net radiation positive) means of monthly forest ($z = 39$ m) and understory ($z = 4$ m) energy balance terms standardized by net radiation (R_n). The last column is the sum of the latent heat (λE), sensible heat (H), soil heat (G_0) and total heat storage (J_t) ratios

Month	R_n (W m^{-2})		$\lambda E/R_n$		H/R_n		G_0/R_n		J_t/R_n		Σ	
	39 m	4 m	39 m	4 m	39 m	4 m	39 m	4 m	39 m	4 m	39 m	4 m
April	257.0	118.4	0.09	0.12	0.63	0.36	0.04	0.09	0.06	0.02	0.82	0.59
May	247.6	95.4	0.20	0.23	0.64	0.51	0.08	0.20	0.05	0.03	0.97	0.97
June	247.3	64.8	0.54	0.53	0.31	0.12	0.05	0.20	0.07	0.06	0.97	0.91
July	268.7	61.6	0.65	0.62	0.20	0.09	0.05	0.20	0.08	0.07	0.98	0.98
August	243.9	58.8	0.59	0.57	0.24	0.08	0.03	0.14	0.09	0.08	0.95	0.87
September	220.6	63.5	0.47	0.31	0.32	0.10	0.03	0.11	0.10	0.06	0.92	0.58

understory level, the short height (0–4 m) precluded any great amount of heat storage, but J_t/R_n ratios still managed to reach 0.03.

Energy balance closure (when $R_n - G_0 - J_t$ equals $\lambda E + H$, energy is balanced or 'closed') was worst in April for both the forest and understory compared to any other month. The pattern of nighttime overestimation and daytime underestimation was pronounced in April, while in May this pattern became less clear. For the understory, the difficulties in estimating R_n with changing solar zenith angles and path lengths were apparent with the sunrise/sunset changes in the energy balance residual. It is not clear why closure was poor in April. It was not strictly due to the presence or absence of leaves, since May had much smaller residuals than April yet the canopies were bare for both months. Although heat storage in the snow pack was not calculated, this should not account for much heat storage given its relatively thin cover and disappearance by April 15, and the energy used to melt ice in the soil was not a large. We hypothesize that the poor closure in April was directly related to the large quantity of H, in that the 1/2 h averaging period was often too short to capture some of the low-frequency eddies associated with the high degree of large-scale convective activity.

4.4.2. Summer (June–July–August)

During the June–July–August full-leaf period, there was no appreciable change in the daytime mean R_n compared to the leafless period. This implies that the increase in reflected solar ($R_s\uparrow$) and emitted long-wave ($R_l\uparrow$) radiation offset the increase in the incident solar radiation ($R_s\downarrow$). Leafless with snow, leafless without snow and leafed $R_s\uparrow/R_s\downarrow$ ratios were 0.20, 0.12 and 0.16, respectively. Between the aspen canopy and the hazelnut, R_n decreased substantially with the development of aspen leaves. The seasonal increase in $R_s\downarrow$ towards the summer solstice was negated by the attenuation of $R_s\downarrow$ through the aspen canopy resulting in an overall decrease in R_n at the hazelnut level.

As expected, the development of transpiring leaf surfaces resulted in an increase in λE largely at the expense of H. Leafed canopy $\lambda E/R_n$ ratios climbed from their bare canopy counterparts to 0.65 for the above-forest values, while similarly climbing to 0.62 for the understory. Despite near similar $\lambda E/H$ ratio at both levels, H/R_n ratios were small beneath the canopy (average 0.10) approximately half that measured above the aspen canopy (average 0.25).

Gradual warming of the soil and shading from the two canopies resulted in a decrease of G_0 with the daytime G_0 typically 0.05 and 0.20 of the overstory or understory R_n, respectively. The total daytime energy (R_n positive) used to heat the air and biomass relative to R_n (at each level) was typically 0.08 for both the forest and hazelnut, similar to the value of 0.06 reported by McCaughey and Saxton (1988) in a mixed temperate forest. Greatest heat storage occurred shortly after sunrise and was comprised largely of heat storage in the boles followed by J_h, J_p, J_e and finally J_l (e.g. daytime mean $J_t = J_b + J_h + J_p + J_e + J_l = 8 + 6 + 5 + 2 + 1$ W m^{-2}). Heat storage in the woody biomass was important especially in the open-canopy structure typical of boreal forest.

Energy balance closure was good during the summer periods, keeping in mind that ensemble averaging removes a lot of variability in the diurnal patterns of the energy balance components. The sum of the daytime energy balance components relative to R_n averaged 0.97 and 0.92 for the forest and understory, respectively.

4.4.3. Late summer–early fall (September)

During September, the decrease in $R_s\downarrow$ and leaf loss resulted in a decrease in R_n at the overstory level. At the understory level, R_n slightly increased due to the removal of leaves from the aspen overstory. As leaf senescence was not as abrupt as leaf emergence, λE decreased somewhat from the summer time values (both levels) while H increased slightly (both levels) lessening the disparity between the two fluxes and returning to energy partitioning patterns similar to June. Continued weakening of soil temperature gradients and the resulting near isothermal temperature profiles kept G_0 small and J_t remained an important component of the energy balance at both levels with typical daytime J_t/R_n ratios of 0.10 (39 m) and 0.06 (4 m). As during April, energy balance closure worsened in September especially at the 4 m level.

4.5. Partitioning overstory and understory turbulent fluxes

The energy balance of this deciduous boreal forest was completely reversed in partitioning between H

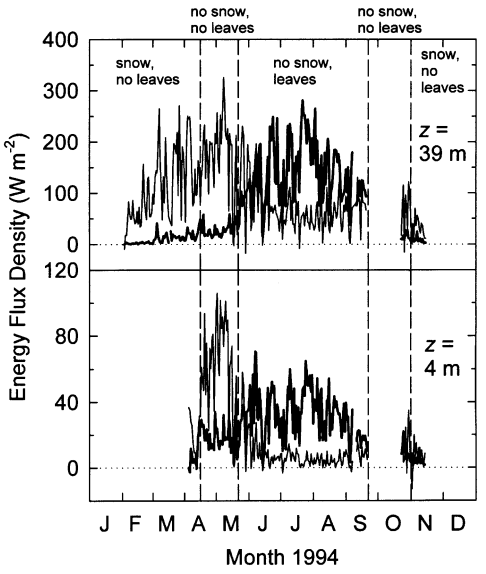

Fig. 10. Seasonal progression of the daytime mean latent heat (thick line) and sensible heat (thin line) fluxes measured above the aspen canopy (39 m) and above the hazelnut understory (4 m). October and November measurements were made in 1993. Vertical dashed lines indicate the dates of changes in the surface conditions noted on the figure (April 15, May 21, September 21 and November 1).

and λE as the leaves developed. This is shown dramatically by the seasonal courses of the daytime mean H and λE not only for the forest as a whole, but also for the understory and forest floor (Fig. 10). With bare canopies and a snow-covered forest floor, H exceeded λE at both heights, and the magnitude of H steadily increased as the winter season progressed. Despite the presence of cold snow on the forest floor, a substantial amount of sensible heat was generated from the forest. During the snow-free, leaf-free period, H continued its steady increase. Now, however, almost half originated from the forest floor. The forest floor also played a larger role in the overall forest λE, as the sharp increase in the surface θ from snowmelt coupled with ample radiation penetration resulted in an increase in soil water evaporation.

The development of leaves saw a concomitant decrease in forest H and an increase in forest λE (daytime means 70 and 139 W m^{-2}, respectively). The wet conditions of 1994, which meant virtually no soil water supply limitation on forest evapotranspiration, resulted in a large λE at the expense of H during the leafed period. Maximum 24 h rates of evapotranspiration equivalent to 5.0–6.0 mm d^{-1} were far above those of nearby boreal mature black spruce (3.0–3.5 mm d^{-1}; Jarvis et al., 1997) and jack pine forests (2.0–2.5 mm d^{-1}; Baldocchi et al., 1997) indicating the large water use by the aspen forest. This sudden transfer of a large volume of water from the substrate to the atmosphere implies that the aspen is indeed a distinct hydrological unit within the boreal forest. This would not only impact the local water cycle, but also would impact the atmosphere's convective boundary layer (CBL). For example, the lack of sensible heat input during the leafed period would result in a shallower, more humid CBL compared to the boreal coniferous forests. Therefore the positive feedback between decreasing canopy conductance and the drying and deepening of the CBL would be weak or absent above the aspen forest, yet strong above the coniferous stands. The difference in CBL heights across the aspen and coniferous stands may also create a breeze blowing from the aspen to the conifer stands.

During the leafed period, the mean daytime λE originating from the hazelnut understory was 33 W m^{-2} and the lysimeter measurements indicated that approximately 7 W m^{-2} (5% of the daytime mean forest λE; 21% of the daytime mean understory λE) was soil water evaporation. The H from the understory during the leafed period was minimal (daytime mean of 8 W m^{-2}). A positive H from the understory often occurred despite an increase in the mean air temperatures with height (inversions) in the aspen canopy, as this is where most radiation was absorbed. As the sensible heat flux normally flows down a temperature gradient (i.e. from high to low temperatures), this within-canopy situation indicates counter-gradient flow, not an uncommon occurrence in forests (Denmead and Bradley, 1985), and especially at night in this forest (see Mahrt et al., 2000). This indicates that intermittent ejections of warm air from the forest floor, capable of breaking through the inversion, were likely to be responsible for most of the positive H from the understory.

Measurements during the fall snow-free, leaf-free period were unfortunately sparse, but it appeared that a repeat of the large springtime snow- and leaf-free H fluxes would not occur. This was presumably due to the low net radiation at this time of year, coupled with

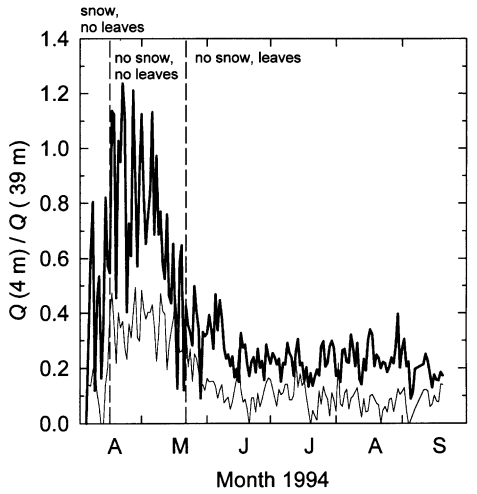

Fig. 11. The ratio of the daytime (net radiation positive) mean latent (thick line) and sensible (thin line) turbulent fluxes measured at the understory level ($z = 4$ m) relative to the overstory level ($z = 39$ m). Vertical dashed lines note the dates of changes in the surface conditions noted on the figure (April 15 and May 21).

the low solar altitude. The presence of snow further reduced the magnitude of both H and λE.

The magnitude of H and λE originating from the hazelnut understory and forest floor relative to the forest can be inferred from Fig. 10, but the role of the understory is more clearly shown by the ratio of the daytime understory-to-overstory turbulent fluxes (Fig. 11). During the leafless period, most of the sensible and latent heat production beneath the overstory originated at the forest floor, whereas after leaf development, most was from the overstory canopy. After snow melt, virtually all of the forest λE was from the forest floor, as λE (4 m)/λE (39 m) approached unity peaking during the snow-free, leaf-free period. Ratios exceeded unity when intercepted snow sublimated from the aspen branches. The H contribution from the forest floor also peaked during this period (H(4 m)/H(39 m) $\approx$ 0.40) as forest floor surface temperatures rose in response to the high solar radiation transmitted through the overstory and drying of the litter layer. The large transpiration rates from the leafed aspen canopy far exceeded that from the understory, decreasing λE (4 m)/λE (39 m) to a steady 0.24 throughout the summer months. The dampening of gust penetration (Blanken et al., 1998) together with an increase in T_a at the aspen canopy level produced weak and sometimes inverted air temperature profiles (mentioned earlier) and hence small sensible heat fluxes from the understory (mean daytime H(4 m)/H(39 m) = 0.10).

4.6. The water balance

The water balance of the forest is given as $P = E + D + \Delta S$ (mm d^{-1}), where E is evapotranspiration, D is vertical drainage, and ΔS is the change in the amount of water stored in the soil. As soil moisture was measured down to a depth of 123 cm (beyond the mean root depth of 60 cm), D is drainage past a depth of 123 cm. The analysis was performed on a daily basis for all of 1994, with extrapolation to periods when measurements were not made. The latter was accomplished using the relationships between measured λE and $R_s\downarrow$ during a period in close seasonal proximity to the extrapolation period. As the extrapolation periods were short and occurred during the winter and late fall when latent heat fluxes were low, errors using these approximations were estimated to be small.

Cumulative totals of the half hourly measured P and E from the forest (aspen + hazelnut + soil), understory (hazelnut + soil) and soil for 1994 are shown in Fig. 12 and summarized in Table 5. As mentioned previously, missing measurements of P for much of January resulted in two estimates of the annual water balance. For each of the P scenarios, E from each level was expressed with and without nighttime low wind speed turbulent heterogeneity and energy balance closure corrections (Blanken et al., 1998). Soil water evaporation was assumed to be 5% of the forest E based on summer lysimeter measurements for all three methods of calculating E.

Several important points concerning the annual water balance can be made. From a methodological standpoint on an annual basis, it did not matter which if any corrections were used to calculate E given the range in the possible total P. Correcting for low nocturnal wind speeds only added 11 mm to the annual forest total and 13 mm at the understory level because E was small at night anyway. The correction for energy balance closure added 21 mm to the annual total forest E but was still within the 20–30 mm uncertainty range in the annual P.

In terms of partitioning, the annual E from the forest between the three components, aspen, hazelnut,

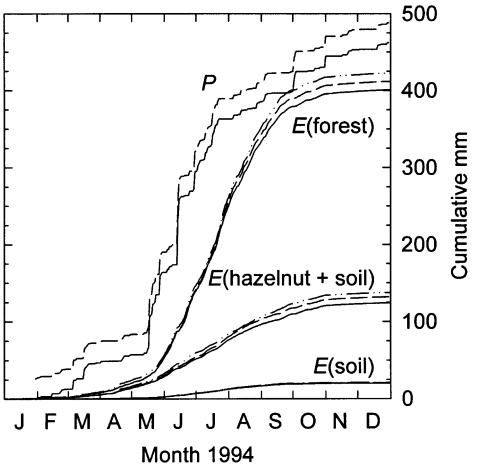

Fig. 12. Cumulative precipitation (P) and evapotranspiration (E) for 1994. The solid line for P does not include part of January preceding gauge installation whereas the dashed line is complete for 1994 with the missing January amount estimated from the thirty-year mean. Evapotranspiration was measured using the eddy-covariance method at the 39 m level (forest E) and 4 m level (hazelnut and soil) with cumulative 1/2 h totals calculated using three methods: (1) not corrected for nighttime underestimation (solid line); (2) corrected for nighttime underestimation (dashed line); and (3) corrected for energy balance closure (dash-dotted line). Soil water evaporation E(soil) (three overlapping lines) was estimated from mid-summer lysimeter measurements which indicated $E(\text{soil}) = 0.05E(\text{forest})$. Periods when measurements were not available were estimated using relationships between E and solar radiation.

and soil accounted for 67–68%, 26–28% and 4–7%, respectively. The fraction of P accounted for by E for the forest as a whole was large (82–91%), where E represents a combination of transpired water, soil water evaporation and the evaporation of intercepted water. The amount of intercepted water evaporated was unknown, however, we suspect it would be a fairly small fraction of the annual P for this continental forest with short, intensive precipitation events.

Over the growing season, starting from when most of the frozen water was melted from the soil (April 20) until senescence (September 20), the change in soil water content was calculated from the volumetric water content (θ) measurements with assignments of θ measurement locations to depths given in Table 6. The surface layers (0–30 cm) showed a net decrease in water content while the deeper layers showed a net increase resulting in an overall net loss of 34.7 mm over the 0–123 cm layer (i.e. $\Delta S = -34.7$ mm. Calculating $\sum(P_i - E_i)\Delta t_i$ using a time step (Δt) of one day (i), for the forest over the same period gave values of between -7.0 and -25.1 mm, depending on corrections to E. The difference between the above estimates of $\sum(P_i - E_i)\Delta t_i$ and the ΔS of -34.7 mm suggested drainage beyond 123 cm over the growing season was small (between 9.6 and 27.7 mm, depending on corrections to E) or 3–8% of the total growing season P of 347 mm. Considering the uncertainty in the $\sum(P_i - E_i)\Delta t_i$ estimate and the measurement of ΔS using one location, we conclude that there was little water movement at the 123 cm depth.

The comparison and courses of measured daily soil

Table 5
Evapotranspiration (E) totals for 1994 for the forest, the hazelnut understory and soil, and the soil alone. See Fig. 12 for measurement and calculation methods. Also shown are the ratios of annual E to annual P (ratios with no parenthesis are for $P = 462.2$ mm, not including January precipitation before gauge installation and ratios within parenthesis are for $P = 488.4$ mm, including missing January precipitation estimated from the thirty-year mean)

Parameter	Source	Calculation method		
		1	2	3
E (mm year^{-1})	Forest	401.1	412.1	422.8
	Hazelnut	124.2	132.0	137.6
	Soil	20.1	20.6	21.1
E/P	Forest	0.87 (0.82)	0.89 (0.84)	0.91 (0.87)
	Hazelnut	0.27 (0.25)	0.29 (0.27)	0.30 (0.28)
	Soil	0.04 (0.04)	0.04 (0.04)	0.05 (0.04)

Table 6
Estimation of the storage of water in the soil profile ($S = \theta\Delta z$) from a depth of 0–123 cm over the period April 20–September 20, 1994. OSP and MSP refer to organic and mineral three-rod horizontal TDR probes, respectively, and ROD (segment number) refers to the vertical segmented TDR rod

TDR probe	Depth assignment (cm)	Δz (cm)	April 20 θ ($m^3\ m^{-3}$)	Initial S (mm)	September 20 θ ($m^3\ m^{-3}$)	Final S (mm)	ΔS (mm)
OSP1	0–10	10	0.50	50.0	0.09	9.0	−41.0
MSP1	10–30	20	0.28	56.0	0.11	22.0	−34.0
ROD1 (3)	30–61	31	0.19	58.9	0.19	58.9	0.0
ROD1 (4)	61–92	31	0.15	46.5	0.20	62.0	15.5
ROD1 (5)	92–123	31	0.26	80.6	0.34	105.4	24.8
Σ	0–123	123	–	292.0	–	257.3	−34.7

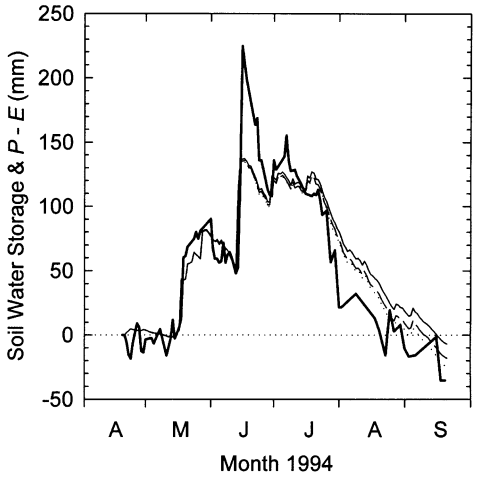

Fig. 13. Soil water storage in the 0–123 cm layer relative to April 20 (initial measured soil water content of 292 mm) determined from volumetric soil moisture measurements (thick line) and cumulative precipitation–evapotranspiration (E) (thin lines) with the eddy flux E uncorrected for nocturnal heterogeneity (solid line), corrected for nocturnal heterogeneity (dashed line) or corrected for energy balance closure (dotted line). The differences between the thick and thin lines are estimates of drainage beyond 123 cm ($D = P - E - \Delta S$).

water storage and $\sum(P_i - E_i)\Delta t_i$ over the April 20–September 20 period is a useful way to examine changes in the soil water balance and the quality of these measurements (Fig. 13). There was remarkably good agreement between the time course of the measured $\sum(P_i - E_i)\Delta t_i$ and S confirming little water flow at the 123 cm depth. Both $\sum(P_i - E_i)\Delta t_i$ and S increased up to mid-June with the persistent May–June rainfall, thereafter decreasing though the remainder of the season. This same pattern of April–June recharge, June–September drawdown, was also observed in 1997 and 1998 using a deep groundwater piezometer (Barr et al., 2000). The heavy June 13 rainfall of 61 mm resulted in the measured storage change exceeding the $\sum(P_i - E_i)\Delta t_i$, presumably due to horizontal movement of water since capillary rise was probably unlikely at this time. During the drying phase, the greater decrease in S than $\sum(P_i - E_i)\Delta t_i$ indicated that there was some water drainage at the 123 cm depth.

5. Summary and conclusions

Anyone asked to imagine the boreal forest is likely

to think of sparse black spruce growing on wet, hummocky terrain covered by lichens and moss with the occasional shrub such as Labrador tea, willow or birch. This image is for the most part correct, however, it should be remembered that approximately 13.5% of the southern boreal forest is covered by extensive aspen stands such as the one described in this study, and another 15.4% is covered by mixed deciduous forests (Hall et al., 1997). Aspen stands are found over a wide range of climactic conditions, but are predominantly found in the cold, continental climates experienced along the southern edge of the North American boreal forest, and alpine regions. The shade-intolerant aspen with its clonal root system enable it to quickly colonize areas disturbed, for example, by fire. It is the deciduous nature of these aspen forests that make them distinct from their coniferous counterparts and the seasonal dynamics of leaf growth and loss have a marked affect on the water and energy exchange.

The presence of aspen stands affects the hydrology and climatolgy for the boreal region in several ways. For example, the high water use by the aspen demands ample water supply and thus places a demand on the regional water supply. The large and sudden onset of water transfer from the substrate to the atmosphere results in shallow, humid CBL compared to the deep, dry CBL over coniferous stands. This, in turn, impacts several other variables including cloud formation, precipitation, surface winds, surface temperature, and the strength of the feedback between the boundary layer and the surface conductance.

Although the results presented here were for a specific year (which was not atypical; see Black et al., 2000) which experienced a wet spring followed by a relatively dry and warm summer, the LAI increase had large effects on the water and energy exchange above and within the forest. The amount of net, photosynthetically active, and solar radiation received at the understory level decreased exponentially as the aspen leaf area increased. Simple effective extinction coefficients calculated from this relationship implied that radiation passed more easily through the leafed than bare aspen canopy due to smaller solar zenith angles, shorter solar-beam path lengths and beam enrichment from forward scattering. The development of leaves was concomitant with an increase in the latent heat flux at the expense of the sensible heat flux. The latent and sensible heat fluxes measured above the hazelnut understory before leafing averaged 67 and 30% (respectively) relative to the forest as a whole, falling to 24 and 10% (respectively) with the presence of leaves. On an annual basis, aspen and hazelnut transpiration accounted for 68 and 27%, respectively, of the total evapotranspiration.

The seasonal water balance was also dependent on leaf development since the relatively high transpiration rates provided a means for soil water depletion. The spring thaw saw a sharp increase in the soil water content in the organic and near-surface mineral horizons. Persistent and often heavy May and June rainfalls were realized as an increase in soil water content as deep as 123 cm. On an annual basis, 82–91% of the precipitation was lost as evapotranspiration from the forest as a whole, while 25–30% and approximately 4% of the annual precipitation was evaporated from the understory and soil, respectively. The agreement between the measured soil water storage and the cumulative difference between precipitation and eddy flux measured evapotranspiration indicated little drainage beyond the rooting zone. Over 200 mm of water was stored in the 0–123 cm soil layer at mid-June, after which soil water was depleted until again reaching the springtime value of 292 mm.

This study has demonstrated the role and seasonal variation of the understory in the overall water and energy exchange of this forest. Even within one season, there was significant variation in the role of the understory, which was largely dependent on the ability of the overstory to attenuate radiation, and the partitioning of soil water between the two levels of vegetation. The latter, we know nothing about, yet it could be an important variable in this study. In addition, we do not know if there are any long-term trends or inter-annual variability in the role of the understory or forest floor relative to the overstory. These could present themselves as long-term trends as the aspen naturally thins as it ages allowing greater radiation penetration or short-term interannual variability as meteorological conditions vary. We therefore encourage researchers to, whenever possible, supplement above- with below-canopy flux measurements in order to fully understand water and energy exchange.

Acknowledgements

The funding was provided by the Natural Sciences and Engineering Research Council of Canada in the form of a four-year collaborative Special Projects and Operating Grant (TAB) and a Postgraduate Scholarship (PDB). Additional support was provided by a University of British Columbia Graduate Scholarship (PDB). The dedicated efforts of many individuals made this research possible: John Deary, Tom Hertzog, Monica Eberle, Mary Dahlman, Paula Pacholek, Murray Heap, Marian Breazu, Mary Yang, Jing Chen, Siguo Chen, Craig Russell, Nigel Livingston, Bill Hook, and Ralph Staebler. The thoughtful comments from the reviewers are greatly appreciated. Finally, we acknowledge the support of our families who endured our absence through the BOREAS project.

References

Baldocchi, D.D., Matt, D.R., Hutchison, B.A., McMillen, R.T., 1984. Solar radiation within an oak-hickory forest: an evaluation of the extinction coefficients for several radiation components during fully-leafed and leafless period. Agricultural and Forest Meteorology 32, 307–322.

Baldocchi, D.D., Vogel, C.A., Hall, B., 1997. Seasonal variation of energy and water vapor exchange rates above and below a boreal jack pine forest canopy. Journal of Geophysical Research 102, 28,939–28,951.

Baldocchi, D.D., Law, B.E., Anthoni, P.M., 2000. On measuring and modeling energy fluxes above the floor of a homogeneous and heterogeneous conifer forest. Agricultural and Forest Meteorology 102, 187–206.

Barr, A.G., van der Kamp, G., Schmidt, R., Black, T.A., 2000. Monitoring the moisture balance of a boreal aspen forest using a deep groundwater piezometer. Agricultural and Forest Meteorology 102, 13–24.

Black, T.A., den Hartog, G., Neumann, H.H., Blanken, P.D., Yang, P.C., Russell, C., Nesic, Z., Staebler, R., Lee, X., Chen, S.C., Staebler, R., Novak, M.D., 1996. Annual cycles of water vapour and carbon dioxide fluxes in and above a boreal aspen forest. Global Change Biology 2, 219–229.

Black, T.A., Chen, W.J., Barr, A.G., Arain, M.A., Chen, Z., Nesic, Z., Hogg, E.H., Neumann, H.H., Yang, P.C., 2000. Increased carbon sequestration by a boreal deciduous forest in years with a warm spring. Geophysical Research Letters 27, 1271–1274.

Blanken, P.D., Black, T.A., Yang, P.C., den Hartog, G., Neumann, H.H., Nesic, Z., Staebler, R., Novak, M.D., Lee, X., 1997. Energy balance and canopy conductance of a boreal aspen forest: partitioning overstory and understory components. Journal of Geophysical Research 102, 28,915–28,927.

Blanken, P.D., Black, T.A., Neumann, H.H., den Hartog, G., Yang, P.C., Nesic, Z., Staebler, R., Chen, W., Novak, M.D., 1998. Turbulent flux measurements above and below the overstory of a boreal aspen forest. Boundary-Layer Meteorology 89, 109–140.

Boast, C.W., Robertson, T.M., 1982. A 'micro-lysimeter' method for determining evaporation from bare soil: description and laboratory evaluation. Soil Science Society of America Journal 46, 689–696.

Brutsaert, W., 1984. Evaporation into the Atmosphere. Reidel, Dordrecht.

Campbell, G.S., Norman, J.M., 1998. An Introduction to Environmental Biophysics. Springer, New York.

Canadian Climate Normals, 1982. Canadian Climate Normals 1951–1980: Temperature and Precipitation, Prairie Provinces. Environment Canada, Ottawa.

Chen, J.M., Blanken, P.D., Black, T.A., Guilbeault, M., Chen, S., 1997. Radiation regime and canopy architecture in a boreal aspen forest. Agricultural and Forest Meteorology 86, 107–125.

Constantin, J., Grelle, A., Ibrom, A., Morgenstern, K., 2000. Flux partitioning between understory and overstory in a boreal spruce/pine forest determined by the eddy covariance method. Agricultural and Forest Meteorology 98–99, 629–643.

Denmead, O.T., Bradley, E.F., 1985. Flux-gradient relationships in a forest canopy. In: Hutchison, B.A., Hicks, B.B. (Eds.). The Forest–Atmosphere Interaction. , pp. 421–442.

Dyer, A.J., 1972. A review of flux–profile relationships. Boundary-Layer Meteorology 7, 363–372.

Fuchs, M., Tanner, C.B., 1968. Calibration and field tests of soil heat flux plates. Soil Science Society of America Proceedings 32, 326–328.

Grant, R.F., Black, T.A., den Hartog, G., Berry, J.A., Neumann, H.H., Blanken, P.D., Yang, P.C., Russell, C., Nalder, I.A., 1999. Diurnal and annual exchanges of mass and energy between an aspen–hazelnut forest and the atmosphere: testing the mathematical model Ecosys with data from the BOREAS experiment. Journal of Geophysical Research 104, 27,699–27,717.

Gu, L.H., Shugart, H.H., Fuentes, J.D., Black, T.A., Shewchuk, S.R., 1999. Micrometeorology, biophysical exchanges and NEE decomposition in a two-story boreal forest — development and test of an integrated model. Agricultural and Forest Meteorology 94, 123–148.

Hall, F.G., Knapp, D.E., Huemmrich, K.F., 1997. Physically based classification and satellite mapping of biophysical characteristics in the southern boreal forest. Journal of Geophysical Research 102, 29,567–29,580.

Hall, F.G., 1999. Introduction to special section: BOREAS in 1999: experiment and science overview. Journal of Geophysical Research 104, 27,627–27,639.

Hare, F.K., Thomas, M.K., 1974. Climate Canada. Wiley, Toronto.

Hayhoe, H.N., Topp, G.C., Bailey, W.G., 1983. Measurement of soil water contents and frozen soil depth during a thaw using time-domain reflectrometry. Atmosphere–Ocean 21, 299–311.

Hillel, D., 1982. Introduction to Soil Physics. Academic Press Inc., San Diego.

Hodges, G.B., Smith, E.A., 1995. Intercalibration, objective analysis, intercomparison and synthesis of BOREAS surface net

radiation measurements. Journal of Geophysical Research 102, 28,885–28,900.

Hook, W.R., Livingston, N.J., 1996. Errors in converting time domain reflectrometry measurements of propagation velocity to estimates of soil water content. Soil Science Society of America Journal 60, 35–41.

Hook, W.R., Livingston, N.J., Sun, Z.J., Hook, P.B., 1992. Remote diode shorting improves measurement of soil water by time domain reflectrometry. Soil Science Society of America Journal 56, 1384–1391.

Jarvis, P.G., Massheder, J.M., Hale, S.E., Moncrieff, J.B., Rayment, M., Scott, S.L., 1997. Seasonal variation of carbon dioxide, water vapour and energy exchanges of a boreal black spruce forest. Journal of Geophysical Research 102, 28,953–28,996.

Leclerc, M.Y., Thurtell, G.W., 1990. Footprint prediction of scalar fluxes using a Markovian analysis. Boundary-Layer Meteorology 52, 247–258.

Lee, X., Barr, A.G., 1998. Climatology of gravity waves in a forest. Quarterly Journal of the Royal Meteorological Society, Part A 124, 1403–1419.

Mahrt, L., Lee, X., Black, A., Neumann, H., Staebler, R.M., 2000. Nocturnal mixing in a forest subcanopy. Agricultural and Forest Meteorology 101, 67–78.

McCaughey, J.H., Saxton, W.L., 1988. Energy balance storage terms in a mixed forest. Agricultural and Forest Meteorology 44, 1–18.

Monsi, M., Saeki, T., 1953. Über der lichtfaktor in den Pfllanzengesell-schaften und seine Bedeutung fur die Stoffprodktion. Japan Journal of Botany 14, 22–52.

Peterson, E.B., Peterson, N.M., 1992. Ecology, management, and use of aspen and balsam poplar in the prairie provinces, Canada. Forestry Canada Northwest Region, Northern Forest Centre, Edmonton, Alberta, Special Report 1.

Rauner, J.U.L., 1976. Deciduous forests. In: Monteith, J.L. (Ed.). Case Studies. Vegetation and the AtmosphereAcademic Press, London, pp. 241–264.

Sellers, P.J., Hall, F.G., Kelly, R.D., Black, A., Baldocchi, D., Berry, J., Ryan, M., Ranson, K.J., Crill, P.M., Lettenmaier, D.P., Margolis, H., Cihlar, J., Newcomer, J., Fitzjarrald, D., Jarvis, P.G., Gower, S.T., Halliwell, D., Williams, D., Goodison, B., Wickland, D.E., Guertin, F.E., 1997. BOREAS in 1997: experiment overview, scientific results, and future directions. Journal of Geophysical Research 102, 28,731–28,769.

Schuepp, P.H., Leclerc, M.Y., MacPerson, J.I., Desjardins, R.L., 1990. Footprint prediction of scalar fluxes from analytical solutions of the diffusion equation. Boundary-Layer Meteorology 50, 355–373.

Spaans, E.A., Baker, J.M., 1995. The soil freezing characteristic: its measurement and similarity to the soil moisture characteristic. Soil Science Society of America Journal 60, 13–19.

Topp, G.C., Davis, J.L., Annan, A.P., 1980. Electromagnetic determination of soil water content: measurements in coaxial transmission lines. Water Resources Research 16, 574–582.

Wilson, K.B., Hanson, P.J., Baldocchi, D.D., 2000. Factors controlling evaporation and energy partitioning beneath a deciduous forest over an annual cycle. Agricultural and Forest Meteorology 102, 83–103.

Yang, P.C., Black, T.A., Neumann, H.H., Novak, M.D., Blanken, P.D., 1999. Spatial and temporal variability of CO_2 concentration and flux in a boreal aspen forest. Journal of Geophysical Research 104, 27,653–27,661.